


Simultaneously Sorting Overlapping Quantum States of Light

Suraj Goel^{✉,*}, Max Tyler^{*}, Feng Zhu, Saroch Leedumrongwattanakun[✉], Mehul Malik[✉], and Jonathan Leach^{✉†}
School of Engineering and Physical Sciences, Heriot-Watt University, Edinburgh, EH14 4AS, United Kingdom

 (Received 15 July 2022; revised 3 October 2022; accepted 21 February 2023; published 6 April 2023)

The efficient manipulation, sorting, and measurement of optical modes and single-photon states is fundamental to classical and quantum science. Here, we realize simultaneous and efficient sorting of nonorthogonal, overlapping states of light, encoded in the transverse spatial degree of freedom. We use a specifically designed multiplane light converter to sort states encoded in dimensions ranging from $d = 3$ to $d = 7$. Through the use of an auxiliary output mode, the multiplane light converter simultaneously performs the unitary operation required for unambiguous discrimination and the basis change for the outcomes to be spatially separated. Our results lay the groundwork for optimal image identification and classification via optical networks, with potential applications ranging from self-driving cars to quantum communication systems.

DOI: [10.1103/PhysRevLett.130.143602](https://doi.org/10.1103/PhysRevLett.130.143602)

Introduction.—The task of discriminating between a set of quantum states is a fundamental requirement in quantum information science, and in particular, quantum communication [1,2]. However, in general, two different quantum states can have a finite, nonzero overlap with respect to each other, making them nonorthogonal and therefore difficult to separate. It is theoretically impossible to perform a measurement that allows us to perfectly distinguish between such states 100% of the time. An important question now follows: given a set of quantum states with a nonzero overlap, what is the best measurement strategy to distinguish between them?

The answer to this question lies in quantum measurement theory, where strategies for the optimal measurement of nonorthogonal quantum states are known [3,4]. In the extreme, we are left with a choice between a measurement strategy that is either efficient or accurate (only orthogonal states can be sorted efficiently and accurately); see Fig. 1. The efficient option is minimum error state discrimination (MESD) [5]. Here, one seeks to perform a set of measurements that categorize every input state. The drawback to MESD is that errors are inevitable, and we have to accept that we will be incorrect with some probability relating to the overlap of the input states. The accurate option is unambiguous state discrimination (USD) [6–10]. Here, one seeks to perform measurements that never incorrectly identify the input state. The downside here is that state identification occurs with a reduced probability; i.e., a measurement does not always provide a result, but when it does, it is always correct. In addition to the extremes, there are intermediate strategies that have been developed that interpolate between MESD and USD. Several theoretical studies include discrimination with a known error margin [11–14], discrimination with a fixed rate of inconclusive outcomes [15–17], and partial state separation with a MESD procedure [18–22].

The problem that we address in this Letter is practical high-dimensional unambiguous state discrimination, i.e., a positive operator-valued measure (POVM) for nonorthogonal, high-dimensional states with simultaneous outcomes. High-dimensional quantum states (or qudits) allow for quantum information to be encoded in a d -dimensional space, enabling quantum communication protocols with increased information capacity and robustness to noise [23–27]. While the theoretical foundation for the necessary measurement strategies has already been developed, their experimental realization has proved to be a significant challenge.

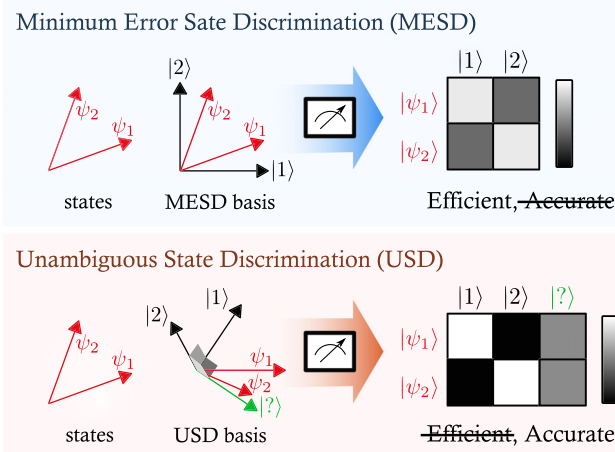


FIG. 1. Measuring nonorthogonal states using minimum error or unambiguous state discrimination. The MESD protocol is efficient in that every input state is always categorized, even if this leads to errors. The USD protocol is accurate in that every input state is correctly identified, even if this does not happen 100% of the time.

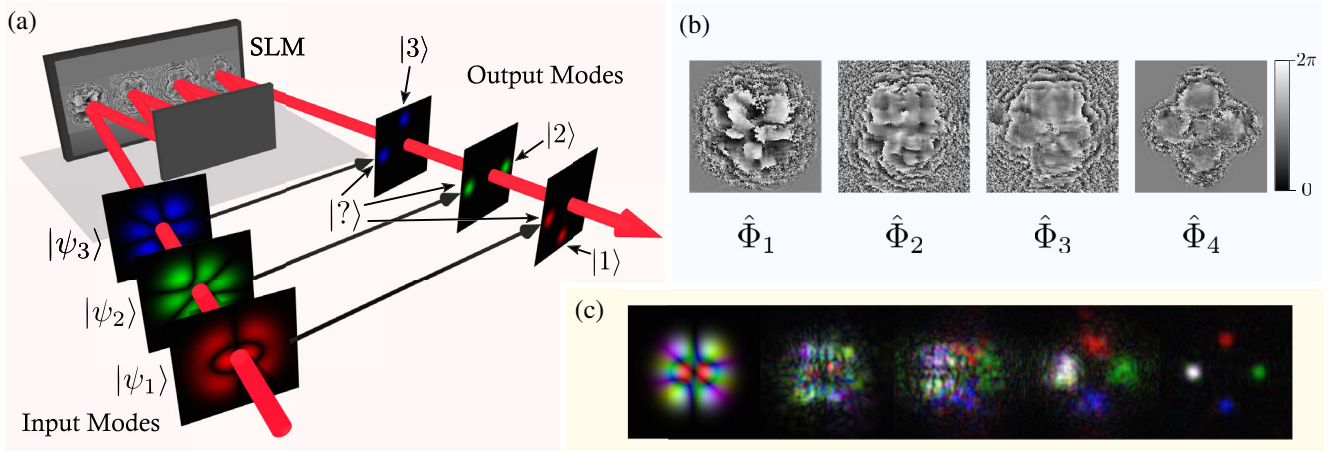


FIG. 2. (a) Schematic of the mode sorter for nonorthogonal states with color used to represent different input modes. The d input modes pass through a multiplane light converter that sorts them into $d + 1$ orthogonal outputs of spatially separated Gaussian spots. The one additional output mode $|?\rangle$ corresponds to the ambiguous outcome. (b) Example holograms used for the MPLC. (c) Amplitudes of nonorthogonal modes as they propagate through the MPLC. SLM, spatial light modulator.

Unambiguous state discrimination was simulated for single-photon states of light encoded in high dimensions using single-outcome projective measurements [28]. Such projective measurements provide a limited functionality in quantum communication systems, where multioutcome measurements are necessary for maximizing key rates and loophole-free tests of Bell nonlocality [29]. Recent Letter on state discrimination includes sorting high-dimensional states using optimal measurement strategies [30], multistate quantum discrimination through optical networks [31], and quantum state elimination [32]. Additionally, much of this recent Letter is related to the complementary field of classical deep optical networks used for information processing and image classification using diffractive optics [33–35]. Methods for sorting and manipulating states using bulk optics [36], two phase screens [37,38], complex media [39–41], and multiplane light converters (MPLCs) [42–49] have been the topic of significant recent research.

The problem we set out to solve in this Letter is the simultaneous sorting of d equally overlapping d -dimensional quantum states of light $\{|\psi_1\rangle, \dots, |\psi_d\rangle\}$, i.e., with all pairwise fidelities of these states equal to each other $F = |\langle \psi_i | \psi_{j \neq i} \rangle|^2$ [10]. There are several requirements in order to perform this task. Firstly, every input mode in the set $\{|\psi_1\rangle, \dots, |\psi_d\rangle\}$ is mapped to an individual measurement mode $\{|1\rangle, \dots, |d\rangle\}$ that uniquely identifies it; i.e., when a photon in state $|\psi_1\rangle$ passes through the system, only the measurement mode $|1\rangle$ can “click.” The challenge is to perform this sorting process when every state in the set has a nonzero fidelity with respect to every other state in the set, i.e., $0 < |\langle \psi_i | \psi_{j \neq i} \rangle|^2 < 1$. Secondly, the system should not make any errors and incorrectly identify any input state; i.e., for the $|\psi_1\rangle$ input state, the probability of all output

modes other than $|1\rangle$ clicking should be equal to zero. Finally, the sorting process occurs simultaneously, and with the highest possible probability, which for USD is given by $\eta = 1 - |\langle \psi_i | \psi_{j \neq i} \rangle|^2$ [10,28].

MPLC for USD.—We realize unambiguous state discrimination within the framework of a multiplane light converter, as shown in Fig. 2. This allows us to simultaneously transform a set of nonorthogonal states in any basis into a new basis of spatially separated measurement modes that can be simultaneously detected by a position-resolving detector. Here, the nonorthogonal states of light we sort are superpositions of Hermite-Gaussian (HG) modes, generated with a spatial light modulator using complex field holograms [50], and we design the output modes of the MPLC to be spatially separated Gaussian spots that can be directly read by a camera or a single-photon detector array. The MPLC is programmed to perform the required unitary (USD operation) and the necessary mode conversion (HG \rightarrow Gaussian spots) at the same time.

The holograms used in MPLC devices are typically constructed using an inverse-design technique known as wave front matching [44,45,51,52]. This is an iterative algorithm where the optical fields for the input and output modes are forward and backward propagated, respectively, and overlapped at each plane of the MPLC. The phase of the MPLC at each plane is calculated in such a way that the entire set of input modes are phase matched to the respective output modes. This process is repeated for each plane sequentially until the algorithm converges and the difference between the forward and backward propagating light is minimized. Each reflection from a mask performs a phase-only transformation $\hat{\Phi}_i$ of the input states of light, which is followed by free-space propagation \hat{H} to the next plane. The total operator of the device after n reflections is

given by $\hat{U} = \hat{H} \prod_{i=n}^1 (\hat{\Phi}_i \hat{H})$. The free-space propagation operator \hat{H} [53,54] is calculated by simulating light propagation in free space as discussed in detail in Supplemental Material [55].

Here we introduce an additional output state labeled $|?\rangle$ into the wave front matching protocol, which means that for d input modes, there are now $d + 1$ output modes. The MPLC device supports a large number of modes, which is ultimately limited by the number of pixels and spatial resolution of the phase masks. The number of modes of the MPLC greatly exceeds the number of modes we sort, which allows us to include the additional auxiliary mode in a straightforward manner. We are free to choose d input modes (superpositions of HG modes) and $d + 1$ output modes (Gaussian spots placed symmetrically on the circumference of a circle). The wave front matching technique then ensures the correct mapping between the two sets of modes.

The purpose of the $|?\rangle$ output is that if a photon is detected in this mode, it provides no information about the input state. However, this also implies that we have not made any incorrect identification, as required by USD. As we can successfully discriminate between any two states with a probability of $1 - F$, the probability that $|?\rangle$ clicks is equal to F . The key to the success of this protocol is that this operator is designed to perform both a unitary operation that maps a set of input states onto the required unambiguous measurement states and simultaneously changes the basis for the measurement outcomes to be spatially separated. Both of these transformations are performed concurrently within the MPLC.

Results.—We performed unambiguous state discrimination for sets of symmetric nonorthogonal states constructed from modes in the Hermite-Gaussian basis. In our experiment, we generated these modes with a HeNe laser and a spatial light modulator, and detected them with a CMOS camera.

In each realisation of USD for high-dimensional states of light, d nonorthogonal modes were transformed into $d + 1$ output modes and measured simultaneously on a CMOS camera. The intensities recorded by the camera pixels located in the output modes were integrated and converted to a detection probability. We achieved USD for sets of states in dimensions ranging from $d = 3$ to 7 for fidelities in the range $F(\psi_i, \psi_{j \neq i}) \in (0, 1)$. Each state was generated as a complex superposition of Hermite-Gauss modes while varying the interstate fidelity from 0 to 1 (see Supplemental Material for further details [55]). The results for USD in seven dimensions are displayed in the form of correlation matrices in Fig. 3. Each row provides its detection probability in all possible outputs. Figure 3(b) compares the experimentally measured probabilities of successful USD to the theoretical predictions. These data clearly demonstrate that unambiguous sorting is achieved for seven-dimensional overlapping states of light.

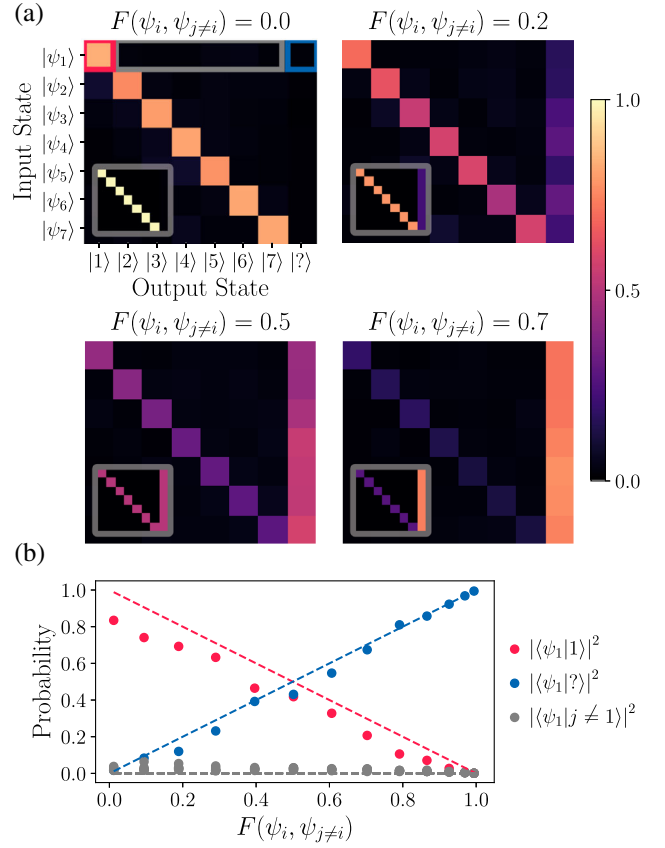


FIG. 3. Measurement data for simultaneous USD in $d = 7$ using a MPLC. (a) Measurement matrices for a range of fidelities (F) between the input states. The insets show the numerically modeled results. The results are normalized by the total power detected in each output state. (b) Probability of measuring an input state $|\psi_1\rangle$ in a given output state $|x\rangle$ as a function of interstate fidelity. This is a cross section of the measurement matrices for the $|\psi_1\rangle$ input state. The points are the measured values, which should be compared to the theoretical predictions, indicated by the dashed lines.

To quantitatively assess our system, we analyze the performance of the MPLC compared to the theoretical limit of minimum error state discrimination [28,56]. No auxiliary state is used in MESD in d dimensions, and the error is instead distributed between the d output states. This leads to a probability of error (p_{err}) in the output, which is defined as the probability of measuring any output state $|j \neq i\rangle$ when given an input state $|\psi_i\rangle$. MESD for uniform-fidelity states has a minimum possible error probability given by $p_{\text{err}} \geq \frac{1}{2} [1 - \sqrt{1 - F(\psi_i, \psi_{j \neq i})}]$ [28,56]. In Fig. 4, we plot the measured error probabilities of our USD protocol against this MESD threshold (gray area). We see that our system outperforms MESD and has a lower error rate than any strategy using MESD over a wide range of interstate fidelities (overlaps). The error probabilities are higher for lower F because the MPLC struggles more when sorting states that are farther apart. Additionally, as d

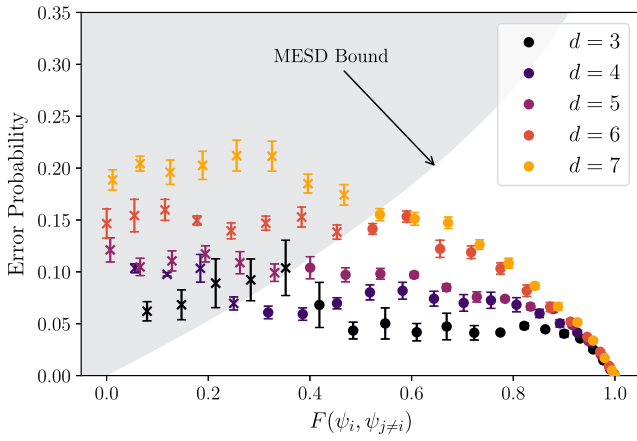


FIG. 4. Evaluation of the MPLC for USD compared to the theoretical limit of MESD. The gray shaded area indicates the error-fidelity region accessible via MESD. Points outside this region represent USD with an error rate that is below than what is possible with MESD.

increases, so too does the total error. The performance reduction of the MPLC for increasing d can be explained as the accuracy of such transformations has been shown to reduce as the dimensionality increases for a fixed number of phase planes [41]. Here, we use four phase planes while increasing the dimensionality of the set of modes that we are sorting. We note that the error rate that we observe is approximately 2 times higher than that of Agnew *et al.* [28], where measurements were performed one outcome at a time, which necessarily includes $(d - 1)/d$ amount of loss. However, in this Letter, all outcomes were measured simultaneously, which is a significant advance over the prior work in terms of practical applications.

Theoretically, the error should be equal to zero for USD, yet we see the experimental implementation using the MPLC performs better for states with a higher initial fidelity (overlap). The reason for this is that as F increases, a higher fraction of the energy is put into the single ambiguous outcome. This mapping, where all input states are sorted to a single output state, is a simpler task to achieve for the MPLC than the case where all input states are sorted to individual outcomes. Additionally, we are comparing our experimental USD implementation to the theoretical limit of MESD. We see that, consequently, there is a region where the error probability does not fall below what MESD could achieve. However, any practical implementation of high-dimensional MESD would be subject to similar error as our experiment and would not perform at this theoretical limit.

Figure 5 shows the extension of our method to the sorting of overlapping images. We sort three images depicting a smiley face, sad face, and neutral face that have a large and symmetric overlap ($F = 0.34$) with respect to each other—the eyes in the images are the same, while the mouth expressions are slightly different, connoting

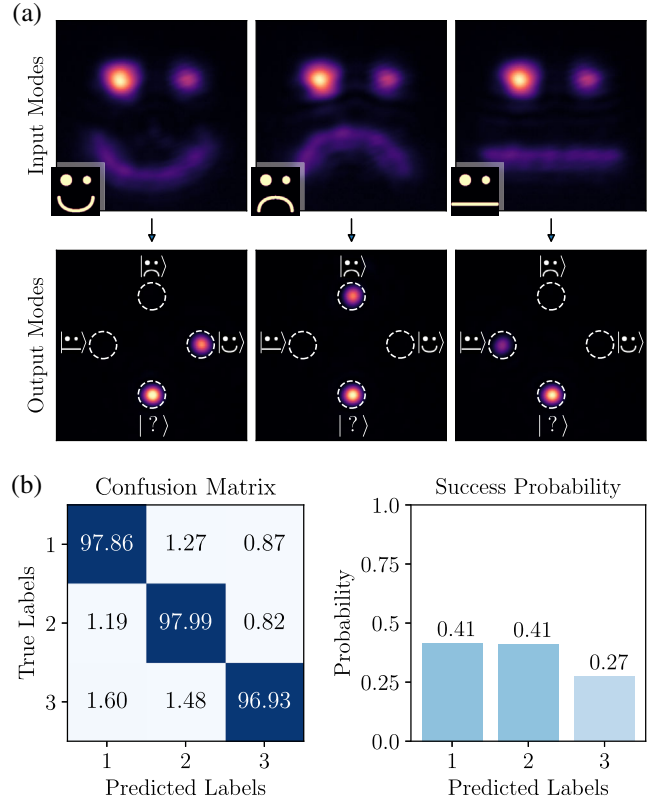


FIG. 5. Sorting overlapping images with the MPLC. The input images have a large fidelity ($F = 0.34$) with each other, yet we can sort them with an accuracy of 97.6%. (a) Shows the measured intensities of the input and output modes. (b) Shows the confusion matrix of the sorting and the associated success probabilities.

completely different emotions. In simple optical image classification, the three faces would be transformed directly to three spatially separated spots, and the wave front matching algorithm would attempt to direct all input light into all output modes, leading to imperfect classification. When using the extra mode $|?\rangle$, we have a place to direct any overlapping light, potentially leading to no errors in our measurement state outputs.

The correlation matrix for the images can be reformatted to a confusion matrix by removing the $|?\rangle$ mode and renormalizing the rows. The success probability for image classification is then calculated as the average ratio of the light intensity in the outcomes of interest compared to the total light intensity of all other outcomes, excluding the ambiguous outcome. Despite the large overlap between the input images, the USD protocol enables the sorting and classification with an average accuracy of 97.6%. We see that the success probability is not constant across all three input states. As numerical simulations suggest that an equal success probability can be obtained, we believe that this asymmetry is due to the combined experimental error of the generation of the input modes and the misalignment between phase masks in the MPLC.

Conclusions.—In this Letter, we solve the measurement problem of simultaneous sorting of high-dimensional non-orthogonal states of light. While previous works simulate a POVM with consecutive measurements, this Letter simultaneously realizes the outcomes of a POVM for high-dimensional nonorthogonal states of light, extending the use of MPLCs to include nonorthogonal input modes. Such simultaneous measurements can also be performed by engineering bases of light that are spatially separable on the detector [57]; however, in this Letter we harness the abilities of MPLC to perform unitary operations in arbitrary spatial bases to perform this task experimentally for the first time.

The key to the success of this protocol is the additional output mode that provides extra flexibility to the system and enables perfect mapping from each of the d non-orthogonal input state to a unique output. The method we adopt is the optimal strategy for minimizing errors and correctly identifying the input states. The consequence of USD is that at the single-photon level, the sorting does not provide an outcome 100% of the time, and for intense modes of light, there is a reduction in the total power that is transmitted into the known output modes. Future Letters will focus on extending our method to sort quantum states and modes that have a nonuniform fidelity with respect to each other, as well as applying such generalized measurement strategies on high-dimensional entangled states of light.

Although this experiment was performed with coherent states of light, the theoretical formalism still applies at the single-photon level since, in the case of linear optics, there is an equivalence between the probabilities associated with single-photon detection and classical laser fields [58]. The extension of our Letter, however, to include multiphoton states is of great interest, and in this case, multiphoton interference can lead to photon bunching or antibunching. For multiphoton inputs, it would be necessary to measure the outcomes of our sorter in coincidence to fully reveal the photon statistics [39,48].

We thank Will McCutcheon for fruitful discussions regarding this work. This work was supported by EPSRC Grants No. EP/T00097X/1 and No. EP/P024114/1, by QuantERA ERA-NET Co-fund (FWF Project No. I3773-N36), and the European Research Council (ERC) Starting grant PIQUaNT (No. 950402).

*These authors contributed equally to this work.

†j.leach@hw.ac.uk

- [1] C. W. Helstrom, *J. Stat. Phys.* **1**, 231 (1969).
- [2] M. A. Nielsen and I. L. Chuang, *Quantum Computation and Quantum Information: 10th Anniversary Edition* (Cambridge University Press, Cambridge, England, 2010).
- [3] S. M. Barnett and S. Croke, *Adv. Opt. Photonics* **1**, 238 (2009).

- [4] A. Chefles, *Contemp. Phys.* **41**, 401 (2000).
- [5] S. M. Barnett and S. Croke, *J. Phys. A* **42**, 062001 (2009).
- [6] I. Ivanovic, *Phys. Lett. A* **123**, 257 (1987).
- [7] A. Chefles and S. M. Barnett, *Phys. Lett. A* **250**, 223 (1998).
- [8] A. Chefles, *Phys. Lett. A* **239**, 339 (1998).
- [9] R. B. M. Clarke, A. Chefles, S. M. Barnett, and E. Riis, *Phys. Rev. A* **63**, 040305(R) (2001).
- [10] S. Franke-Arnold and J. Jeffers, *Eur. Phys. J. D* **66**, 196 (2012).
- [11] A. Hayashi, T. Hashimoto, and M. Horibe, *Phys. Rev. A* **78**, 012333 (2008).
- [12] H. Sugimoto, T. Hashimoto, M. Horibe, and A. Hayashi, *Phys. Rev. A* **80**, 052322 (2009).
- [13] H. Sugimoto, Y. Taninaka, and A. Hayashi, *Phys. Rev. A* **86**, 042311 (2012).
- [14] G. Sentís, E. Bagan, J. Calsamiglia, and R. Muñoz Tapia, *Phys. Rev. A* **88**, 052304 (2013).
- [15] E. Bagan, R. Muñoz Tapia, G. A. Olivares-Rentería, and J. A. Bergou, *Phys. Rev. A* **86**, 040303(R) (2012).
- [16] U. Herzog, *Phys. Rev. A* **86**, 032314 (2012).
- [17] O. Jiménez, M. A. Solís-Prosser, L. Neves, and A. Delgado, *Entropy* **23**, 73 (2021).
- [18] K. Nakahira, T. S. Usuda, and K. Kato, *Phys. Rev. A* **86**, 032316 (2012).
- [19] K. Nakahira, T. S. Usuda, and K. Kato, *Phys. Rev. A* **91**, 022331 (2015).
- [20] K. Nakahira, K. Kato, and T. S. Usuda, *Phys. Rev. A* **92**, 059901(E) (2015).
- [21] M. A. Solís-Prosser, A. Delgado, O. Jiménez, and L. Neves, *Phys. Rev. A* **93**, 012337 (2016).
- [22] K. Nakahira, T. S. Usuda, and K. Kato, *IEEE Trans. Inf. Theory* **63**, 7845 (2017).
- [23] M. Mirhosseini, O. S. Magaña-Loaiza, M. N. O’Sullivan, B. Rodenburg, M. Malik, M. P. J. Lavery, M. J. Padgett, D. J. Gauthier, and R. W. Boyd, *New J. Phys.* **17**, 033033 (2015).
- [24] M. Pivoluska, M. Huber, and M. Malik, *Phys. Rev. A* **97**, 032312 (2018).
- [25] F. Zhu, M. Tyler, N. H. Valencia, M. Malik, and J. Leach, *AVS Quantum Sci.* **3**, 011401 (2021).
- [26] S. Ecker, F. Bouchard, L. Bulla, F. Brandt, O. Kohout, F. Steinlechner, R. Fickler, M. Malik, Y. Guryanova, R. Ursin, and M. Huber, *Phys. Rev. X* **9**, 041042 (2019).
- [27] V. Srivastav, N. H. Valencia, W. McCutcheon, S. Leedumrongwathanakun, S. Designolle, R. Uola, N. Brunner, and M. Malik, *Phys. Rev. X* **12**, 041023 (2022).
- [28] M. Agnew, E. Bolduc, K. J. Resch, S. Franke-Arnold, and J. Leach, *Phys. Rev. Lett.* **113**, 020501 (2014).
- [29] B. G. Christensen, K. T. McCusker, J. B. Altepeter, B. Calkins, T. Gerrits, A. E. Lita, A. Miller, L. K. Shalm, Y. Zhang, S. W. Nam, N. Brunner, C. C. W. Lim, N. Gisin, and P. G. Kwiat, *Phys. Rev. Lett.* **111**, 130406 (2013).
- [30] M. Solís-Prosser, O. Jiménez, A. Delgado, and L. Neves, *Quantum Sci. Technol.* **7**, 015017 (2021).
- [31] A. Laneve, A. Gherardi, F. Hamiti, P. Mataloni, and F. Caruso, *Quantum Sci. Technol.* **7**, 025028 (2022).
- [32] J. W. Webb, I. V. Puthoor, J. Ho, J. Crickmore, E. Blakely, A. Fedrizzi, and E. Andersson, [arXiv:2207.00019](https://arxiv.org/abs/2207.00019).
- [33] X. Lin, Y. Rivenson, N. T. Yardimci, M. Veli, Y. Luo, M. Jarrahi, and A. Ozcan, *Science* **361**, 1004 (2018).

- [34] G. Wetzstein, A. Ozcan, S. Gigan, S. Fan, D. Englund, M. Soljačić, C. Denz, D. A. B. Miller, and D. Psaltis, *Nature (London)* **588**, 39 (2020).
- [35] O. Kulce, D. Mengu, Y. Rivenson, and A. Ozcan, *Light Sci. Appl.* **10**, 25 (2021).
- [36] J. Leach, M. J. Padgett, S. M. Barnett, S. Franke-Arnold, and J. Courtial, *Phys. Rev. Lett.* **88**, 257901 (2002).
- [37] G. C. G. Berkhout, M. P. J. Lavery, J. Courtial, M. W. Beijersbergen, and M. J. Padgett, *Phys. Rev. Lett.* **105**, 153601 (2010).
- [38] M. Mirhosseini, M. Malik, Z. Shi, and R. W. Boyd, *Nat. Commun.* **4**, 2781 (2013).
- [39] H. Defienne, M. Barbieri, I. A. Walmsley, B. J. Smith, and S. Gigan, *Sci. Adv.* **2**, e1501054 (2016).
- [40] S. Leedumrongwatthanakun, L. Innocenti, H. Defienne, T. Juffmann, A. Ferraro, M. Paternostro, and S. Gigan, *Nat. Photonics* **14**, 139 (2020).
- [41] S. Goel, S. Leedumrongwatthanakun, N. H. Valencia, W. McCutcheon, C. Conti, P. W. Pinkse, and M. Malik, *arXiv:2204.00578*.
- [42] J. F. Morizur, L. Nicholls, P. Jian, S. Armstrong, N. Treps, B. Hage, M. Hsu, W. Bowen, J. Janousek, and H. A. Bachor, *J. Opt. Soc. Am. A* **27**, 2524 (2010).
- [43] G. Labroille, B. Denolle, P. Jian, P. Genevoux, N. Treps, J. F. Morizur, P. Genevoux, and N. Treps, *Opt. Express* **22**, 15599 (2014).
- [44] N. K. Fontaine, R. Ryf, H. Chen, D. Neilson, and J. Carpenter, in *Proceedings of the 2017 European Conference on Optical Communication (ECOC)* (IEEE, 2017), pp. 1–3.
- [45] N. K. Fontaine, R. Ryf, H. Chen, D. T. Neilson, K. Kim, and J. Carpenter, *Nat. Commun.* **10**, 1865 (2019).
- [46] M. Mounaix, N. K. Fontaine, D. T. Neilson, R. Ryf, H. Chen, J. C. Alvarado-Zacarias, and J. Carpenter, *Nat. Commun.* **11**, 5813 (2020).
- [47] F. Brandt, M. Hiekkamäki, F. Bouchard, M. Huber, and R. Fickler, *Optica* **7**, 98 (2020).
- [48] M. Hiekkamäki and R. Fickler, *Phys. Rev. Lett.* **126**, 123601 (2021).
- [49] O. Lib, K. Sulimany, and Y. Bromberg, *Phys. Rev. Appl.* **18**, 014063 (2022).
- [50] V. Arrizón, G. Méndez, and D. S. de La-Llave, *Opt. Express* **13**, 7913 (2005).
- [51] T. Hashimoto, T. Saida, I. Ogawa, M. Kohtoku, T. Shibata, and H. Takahashi, *Opt. Lett.* **30**, 2620 (2005).
- [52] Y. Sakamaki, T. Saida, T. Hashimoto, and H. Takahashi, *J. Lightwave Technol.* **25**, 3511 (2007).
- [53] A. Siegman, *Lasers* (University Science Books, Mill Valley, CA, 1986).
- [54] K. Khare, *Fourier Optics and Computational Imaging* (John Wiley & Sons, New York, 2015).
- [55] See Supplemental Material at <http://link.aps.org/supplemental/10.1103/PhysRevLett.130.143602> contains further information on the experimental procedure, the wavefront matching, and additional supporting data.
- [56] D. Qiu, *Phys. Rev. A* **77**, 012328 (2008).
- [57] M. A. Solís-Prosser, M. F. Fernandes, O. Jiménez, A. Delgado, and L. Neves, *Phys. Rev. Lett.* **118**, 100501 (2017).
- [58] S. M. Barnett, *Phys. Scr.* **97**, 114004 (2022).